JOURNAL OF AIRCRAFT
Vol. 41, No. 4, July–August 2004

Novel Two-Dimensional Modeling Approach for Aircraft Icing

Krzysztof Szilder*
National Research Council, Ottawa, Ontario K1A 0R6, Canada
and
Edward P. Lozowski†
University of Alberta, Edmonton, Alberta T6G 2E3, Canada

A new modeling approach to tackle the challenging problem of in-flight icing prediction is formulated and verified. With use of this new approach, termed morphogenetic modeling, the shape, structural details, and density of aircraft ice accretions are predicted by emulating the behavior of individual fluid elements. A two-dimensional, morphogenetic model is used to predict the ice accretion forming on a cylinder over a range of in-flight conditions. The model predicts rime, glaze, and simultaneous glaze and rime accretions. A partial verification of the model has been successfully accomplished. Although there are some discrepancies between experimental and predicted accretion shapes, especially for large and wet accretions, the overall agreement is good. In particular, the prediction of the stagnation line growth rate agrees well with experimental data. The results of our exploratory research are encouraging and suggest that morphogenetic modeling has the potential to advance the simulation of in-flight icing. Practical implementation of this approach will require coupling the model to an external flowfield solver, as well as to heat transfer and droplet impingement solvers. Further verification and extension to three dimensions are planned.

Nomenclature

c_P	=	specific heat capacity of dry air at constant pressure, $J \cdot kg^{-1} \cdot K^{-1}$
c_W	=	specific heat capacity of water, $J \cdot kg^{-1} \cdot K^{-1}$
e_S, e_A	=	saturation vapor pressure at T_S and T_A, respectively, Pa
h	=	convective heat transfer coefficient, $W \cdot m^{-2} \cdot K^{-1}$
k_A	=	thermal conductivity of air, $W \cdot m^{-1} \cdot K^{-1}$
L_F	=	specific latent heat of freezing, $J \cdot kg^{-1}$
L_V	=	specific latent heat of vaporization, $J \cdot kg^{-1}$
M_{Fj}	=	freezing mass flux per unit length at location j, $kg \cdot m^{-1} \cdot s^{-1}$
M_{WVi}	=	impinging water mass flux on a vertical surface segment per unit length at location i, $kg \cdot m^{-1} \cdot s^{-1}$
m	=	water mass flux along the surface, $kg \cdot m^{-1} \cdot s^{-1}$
m_F	=	freezing mass flux, $kg \cdot m^{-2} \cdot s^{-1}$
m_W	=	impinging water mass flux, $kg \cdot m^{-2} \cdot s^{-1}$
Nu	=	Nusselt number
P_n	=	freezing probability
Pr	=	Prandtl number
p	=	static pressure in the freestream, Pa
Q_C	=	convective heat flux, $W \cdot m^{-2}$
Q_E	=	evaporative heat flux, $W \cdot m^{-2}$
Q_F	=	latent heat flux, $W \cdot m^{-2}$
Q_V	=	aerodynamic heating flux, $W \cdot m^{-2}$
Q_W	=	sensible heat flux of the impinging droplets, $W \cdot m^{-2}$
R	=	cylinder radius, m
Re	=	Reynolds number, $2RU/\nu$
r	=	median-volume radius of the droplet spectrum, μm
r_C	=	local recovery factor
S	=	runback factor
Sc	=	Schmidt number
T_A	=	air temperature, K
T_S	=	accretion surface temperature, K
U	=	uniform airstream velocity, $m \cdot s^{-1}$
V	=	droplet impact speed, $m \cdot s^{-1}$
W	=	airstream liquid water content, $kg \cdot m^{-3}$
α	=	azimuth angle measured from the stagnation point, rad
α_M	=	maximum impingement angle, rad
α_R	=	maximum runback angle, rad
β	=	local collision efficiency
Δl	=	lattice cell size, m
Δs	=	discrete length measured along the surface, m
ε	=	ratio of the molecular weights of water vapor and dry air
ν	=	kinematic viscosity of air, $m^2 \cdot s^{-1}$
ρ_I	=	ice density, $kg \cdot m^{-3}$

Subscripts

i, j, n, m	=	indicate discrete locations on the accretion surface
V	=	vertical
0	=	stagnation line

Introduction

A VARIETY of numerical ice accretion models have been developed by research groups based in companies, research organizations, and universities around the world.[1–4] Despite differences among the models, they all consist of the following four principal elements: 1) determination of the airflow around the body of interest, 2) calculation of supercooled water droplet trajectories and/or determination of the liquid impingement distribution over the body, 3) thermal energy analysis of the air–water–ice–surface system that determines the local rate of ice growth and the flux of water film flow on the surface, and 4) determination of the evolving ice shape. Depending on the complexity of the ice accretion model, a system of partial or ordinary differential equations, along with appropriate boundary and initial conditions, constitutes its mathematical framework. We perceive that, in general, there is no clear relationship between a model's mathematical complexity and its accuracy in reproducing experimental results. It appears that existing models do

Presented as Paper 2003-1075 at the AIAA 41st Aerospace Sciences Meeting and Exhibit, Reno, NV, 6 January 2003; received 13 January 2003; revision received 12 May 2003; accepted for publication 13 May 2003.

*Research Officer, Aerodynamics Laboratory, Institute for Aerospace Research; Krzysztof.Szilder@nrc-cnrc.gc.ca. Member AIAA.

†Professor, Department of Earth and Atmospheric Sciences; Edward.Lozowski@ualberta.ca.

adequately predict rime ice growth.[5,6] In addition, recently Myers et al.[7] have proposed a theoretical model that focuses on computing the surface liquid flow and glaze ice growth.

It is well known that, under certain icing conditions, the growth of rime feathers may occur downstream from glaze ice. Rime feathers are characterized by instantaneous solidification of the impinging droplets (or at least the formation of a mechanically robust ice shell), whereas a water layer covers the glaze ice surface that forms upstream. Whereas rime feathers are strictly speaking a three-dimensional phenomenon, a two-dimensional analog can be simulated with the present model. To the best of our knowledge, a comprehensive model capable of simulating the coexistence of these two types of icing has not yet been published, although some progress has been made toward this goal.[8]

The goal of our research has been to work toward a new paradigm in aircraft icing modeling. In this paper, we will introduce and validate a novel, discrete particle model. This two-dimensional model is capable of simulating icing over a range of in-flight icing conditions, including coexisting glaze and rime icing. We call this approach to icing modeling morphogenetic modeling. Morphogenetic modeling was introduced by Szilder[9] who used a discrete, random walk method to simulate ice accretion on a two-dimensional cylinder due to freezing rain. Since then we have successfully used the morphogenetic approach to simulate ice density at the stagnation region in two-dimensional[10] and three-dimensional[11] simulations. Three-dimensional ice accretion shapes forming on objects of various geometries have also been investigated.[12,13] However, until now, the model has been applied primarily to the prediction of icing on electrical power transmission lines and insulators.

Ice Accretion Model

The two-dimensional morphogenetic model presented here is an enhanced version of the model described by Szilder[9] and Szilder et al.[14] It was developed originally for freezing rain applications. Two essential features have been introduced since then: first, a distribution of local collision efficiency and, second, a distribution of heat transfer over the icing surface. Our first attempt to simulate in-flight glaze icing with constant density was reported by Szilder and Lozowski.[15] In this paper, we focus on the coexistence of glaze and rime icing regimes. We will examine the predicted distribution of ice density and undertake a partial experimental verification of the model. Before describing our implementation of the discrete particle method, we begin by summarizing the underlying theory.

Because the model has not yet been coupled to a droplet trajectory model, we parameterize the effect of local collision efficiency by imposing the following distribution of impinging water mass flux,[15]

$$m_W = UW\beta_0 \cos[(\pi/2)(\alpha/\alpha_M)] \qquad \text{for} \qquad 0 \le \alpha \le \alpha_M \tag{1}$$

The stagnation point collision efficiency and the maximum impingement angle are considered to be functions of the airspeed, droplet size, and cylinder radius as in Ref. 16. Qualitatively, this means that an increase of either the airstream velocity or the droplet diameter leads to an increase of the stagnation line collision efficiency and the maximum impingement angle, for a given cylinder radius.

We assume that the physical processes occurring on the ice surface are governed by a steady-state heat balance written in the form:

$$Q_F = Q_C + Q_E + Q_V + Q_W \tag{2}$$

The latent heat of freezing is given by

$$Q_F = L_F m_F \tag{3}$$

The convective heat flux is given by

$$Q_C = h(T_S - T_A) \qquad \text{where} \qquad h = k_A Nu/2R$$

$$Nu = Re^{0.5}[2.4 - 1.2\cos(3.6\alpha)] \tag{4}$$

The expression for the Nusselt number distribution is a fit to experimental data for a rough cylinder used by Lozowski et al.[16]

The evaporative heat flux is given by

$$Q_E = h(Pr/Sc)^{0.63}\varepsilon L_V/pc_P(e_S - e_A) \tag{5}$$

The aerodynamic heating term, Q_V is given by

$$Q_V = -hr_C U^2/2c_p \qquad \text{where} \qquad r_C = 0.75 + 0.25\cos(2\alpha) \tag{6}$$

The sensible heat flux between the impinging droplets and the accretion is given by

$$Q_W = m_W c_W (T_S - T_A) \tag{7}$$

Sublimation has been ignored, in accordance with the findings of Lozowski et al.[16] Equation (2), in conjunction with Eqs. (3–7) and specified atmospheric conditions, may be solved for the freezing mass flux m_F or the surface temperature T_S. Two cases may be distinguished: glaze ice when $T_S = 0°\text{C}$ and the freezing mass flux is calculated and rime ice when $m_F = m_W$ and the surface temperature T_S is calculated. So far, the model is fairly conventional.

The shape of the resulting glaze ice accretion is determined, in part, by the extent of the runback. To quantify this effect, we introduce a dimensionless runback factor S. It is the ratio of the impinging mass flux to the freezing mass flux at the stagnation line:

$$S = \frac{m_W(\alpha = 0)}{m_F(\alpha = 0)} \tag{8}$$

When $S = 1$, all impinging water freezes on impact at the stagnation line, forming rime ice in its vicinity. When $S > 1$, unfrozen water flows downstream from the stagnation line, forming glaze ice from the stagnation line to a certain maximum runback angle α_R. Rime ice may grow beyond α_R. The runback factor may be rewritten using Eqs. (1–3) as

$$S = \frac{UW\beta_0 L_F}{Q_F(\alpha = 0)} \tag{9}$$

We now summarize the main characteristics of the morphogenetic model. In the following sections on glaze ice and rime ice, we will focus on specific model characteristics for each regime. Overall, however, the morphogenetic model, as implemented here, is a random walk model that emulates the motion and freezing of discrete fluid elements. A model fluid element may be imagined to consist of an ensemble of cloud droplets, all of which undergo identical histories. A two-dimensional square lattice defines the accretion domain. Because at present we lack coupled airflow and droplet trajectory models, we constrain the morphogenetic model so that there is no updating of the heat transfer or collision efficiency during ice growth. Consequently, the model in its present form is strictly applicable only to early ice growth.

Fluid elements impact randomly on the cylinder surface or on the existing ice structure, in such a way that their distribution, on impact, accords with the following equation:

$$\beta = \beta_0 \cos[(\pi/2)(\alpha/\alpha_M)] \tag{10}$$

Following impact, each fluid element begins a random walk from grid cell to grid cell, moving downstream along the surface, from its initial impact location (Fig. 1). At each step in the process, using a FORTRAN library subroutine, a pseudorandom number is generated, having a uniform distribution between zero and unity. This random number is compared with the probability of freezing that will be introduced in the next section. Depending on the result of this comparison, the element either freezes or moves to an adjacent grid cell. Naturally, freezing occurs only if there is sufficient heat transfer to the subfreezing airstream.

The model is sequential, so that, as soon as a particular fluid element freezes, the behavior of the next element is considered. Simulations of fluid element motion and freezing are performed consecutively for the total number of fluid elements determined by the total intercepted mass flux.

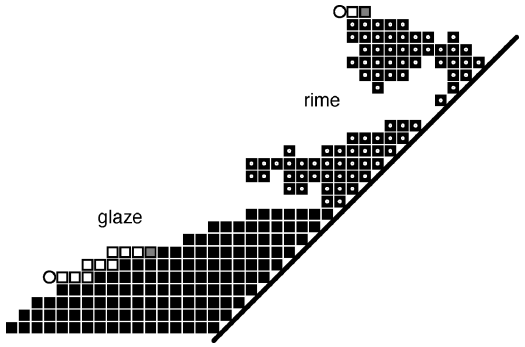

Fig. 1 Morphogenetic prediction: ■, glaze; ◘, rime; ○, impinging particles on glaze and rime ice; □, locations visited by the moving fluid particle; and ■, final resting location.

Glaze Icing Submodel

Glaze ice occurs where there is surface liquid flow. As earlier, we will begin with the underlying theory and then describe its numerical implementation. We first consider the mass conservation equation for steady water flow over the upstream half of the cylinder, $0 \le \alpha \le \frac{1}{2}\pi$. Symmetry above and below the stagnation line is imposed because gravitational effects are neglected. To keep the model simple, we assume that once a fluid element hits the cylinder surface (without splashing), it flows downstream along the surface. It is further assumed that any unfrozen water is shed from the cylinder at $\alpha = \frac{1}{2}\pi$. The variation of the water mass flux along the cylinder surface is, therefore, determined by the difference between the impinging water flux and the freezing mass flux:

$$\frac{\mathrm{d}m}{\mathrm{d}\alpha} = [m_W(\alpha) - m_F(\alpha)]R \tag{11}$$

Integration of Eq. (11) gives the variation of the water mass with azimuthal angle. The location where this water mass flux diminishes to zero is defined as the maximum runback angle α_R:

$$\int_0^{\alpha_R} [m_W(\alpha) - m_F(\alpha)]\,\mathrm{d}\alpha = 0 \tag{12}$$

The solution of Eq. (12) gives the maximum runback angle as a function of atmospheric conditions. Three cases may be distinguished: $\alpha_R = 0$, rime icing occurs everywhere where droplets impinge ($0 \le \alpha \le \alpha_M$); $0 < \alpha_R < \alpha_M$, glaze appears downstream from the stagnation line ($0 \le \alpha \le \alpha_R$) and rime forms downstream from the maximum runback angle ($\alpha_R \le \alpha \le \alpha_M$); and $\alpha_M \le \alpha_R$, glaze forms over the entire accretion ($0 \le \alpha \le \alpha_R$).

We now derive a relation for the freezing probability as a function of the controlling macroscopic physical variables. We examine the nth lattice site measured downstream from the stagnation line along the discretized cylinder or accretion surface. We consider that the mass flux of impinging water on a vertical surface segment, per unit length of the cylinder, M_{WVi}, decreases from its maximum value at the stagnation line to zero at the maximum impingement location. In addition, we take the impinging mass flux to be zero on horizontal surface segments and also on all segments downstream from the maximum impingement location. The freezing rate per unit length, M_{Fj}, varies with location, and freezing may occur on both horizontal and vertical surface segments. Consequently, the mass of water entering the nth site is given by the difference between the total upstream impinging water mass,

$$\sum_{i=1}^{m} M_{WVi}$$

(where m is the number of upstream vertical surface segments), and the total mass frozen upstream,

$$\sum_{j=1}^{n-1} M_{Fj}$$

Note that $m \le n$, because the discrete approximation of the cylinder or accretion surface by the boundaries of square grid cells produces a staircase surface profile, with some grid sites where fluid elements cannot impinge directly, although they may freeze there, for example, horizontal surface segments. If the freezing rate at the nth site is M_{Fn}, we set the freezing probability equal to the ratio of the mass frozen at site n to the incoming liquid mass at the site:

$$P_n = M_{Fn} \Bigg/ \left(\sum_{i=1}^{m} M_{WVi} - \sum_{j=1}^{n-1} M_{Fj} \right) \tag{13}$$

This means that the microscopic local freezing probability is set equal to the macroscopic local freezing fraction. The morphogenetic model values of M_{WVi} and M_{Fj} may be related to the physical value of the impinging water mass flux on vertical surfaces, m_{WVi}, and the freezing rate m_{Fj} as follows:

$$M_{WVi} = m_{WVi}\Delta l, \qquad M_{Fj} = m_{Fj}\Delta s_j \tag{14}$$

where m_{WVi} is related to the impinging water mass flux according to $m_{Wi} = m_{WVi}\cos(\alpha_i)$ and α_i is the angle between the mean droplet impingement direction and the normal to the cylinder surface. The dimension Δl is the grid cell size, and Δs_j is the discrete length measured along the surface between grid cell centers at sites $j-1$ and j. Substituting the expressions from Eq. (14) into Eq. (13) gives a relation for the freezing probability at site n,

$$P_n = \Delta s_n \Bigg/ \left(\Delta l \sum_{i=1}^{m} S_{i,n} - S_{1,n} \sum_{j=1}^{n-1} \frac{\Delta s_j}{S_{1,j}} \right)$$

$$\text{where} \quad S_{i,j} = \frac{m_{WVi}}{m_{Fj}}, \qquad n = 1, 2, \ldots, n_t, \qquad m \le n \tag{15}$$

where n_t is the total number of segments measured along the discrete surface, from the stagnation line to the shedding location. The local runback factor, $S_{i,j}$, defined as the ratio of local impinging and freezing fluxes, may be expressed using Eqs. (1-3) and (9) as a function of azimuth and the runback factor at the stagnation line:

$$S_{i,j} = \frac{UW\beta_0 \cos[(\pi/2)(\alpha_i/\alpha_M)]/\cos(\alpha_i)}{Q_F(\alpha_j)/L_F}$$

$$= S\frac{\cos[(\pi/2)(\alpha_i/\alpha_M)]}{\cos(\alpha_i)} \frac{Q_F(\alpha = 0)}{Q_F(\alpha_j)} \tag{16}$$

Before launching each new fluid element, a new distribution of the freezing probability along the evolving surface is calculated using Eqs. (15) and (16). To accomplish this task, the accretion is divided into upper and lower sections, as determined by the location of the stagnation point. This allows us to ensure correspondence between the direction of fluid element motion along the cylinder or ice accretion surface and the direction of the adjacent airflow. This recalculation of the distribution of freezing probability, before to considering the motion of the next fluid element, allows the effect of the changing accretion shape on the runback and freezing processes to be taken into account, at least in part. For now, we use Eq. (4) to specify the distribution of the heat transfer coefficient throughout the growth. Hence, the direct effect of a changing accretion shape on the local heat transfer coefficient is not considered, for example, enhanced heat transfer over surface protrusions or horns.

Each fluid element ends its motion either by freezing or by shedding while still in a liquid state. A fluid element is considered to freeze if the pseudorandom number generated for a particular step is less than or equal to the local freezing probability, specified by Eq. (15). When a fluid element freezes, a cradle location is sought in the neighborhood of the freezing grid cell. This neighborhood is a circle centered on the initially determined freezing point with a radius equal to $5\Delta l$ (Szilder[9]). The freezing fluid element is moved

to the empty cell within this domain, where it will have the maximum number of occupied neighbors. If there is more than one such location, the final site is chosen randomly from among them, assuming an equal probability of allocation to each site. The purpose in seeking a cradle site for the final fluid element resting location is to emulate the effect of surface tension in producing a relatively compact and smooth ice accretion.

Rime Icing Submodel

Rime icing is considered to occur in the model at locations where there is no surface liquid flow. Morphogenetic models of the internal structure and density of rime in two and three dimensions have been published by Szilder[10] and Szilder and Lozowski.[11] In these papers, the droplets were considered to impinge perpendicularly on a flat surface. This section is an extension of this previous work, where droplets may impinge at various angles either on a bare cylinder or on an ice-covered cylinder.

Macklin[17] has argued that the density of accreted ice depends on the ratio of the momentum of the impacting droplets (proportional to r^3V) to the strength of the ice bond (which varies as r^2). In addition, he contends that the density also depends on the freezing time, which, to a first approximation, varies inversely with the surface temperature T_S expressed in degrees Celsius. Consequently, he suggested that the accretion density might be expressed as a function of the parameter $rV(-T_S)^{-1}$, now called the Macklin parameter.

There is a body of experimental results that relate the Macklin parameter to ice density. However, we have not encountered an explicit relation to predict ice accretion density variation with azimuthal angle on a cylinder. Consequently, we will employ, for the entire impingement area, the following relation obtained for the stagnation line of a fixed cylinder.[18]

$$\rho_I = 280(rV/-T_S)^{0.6} \tag{17}$$

When the variation of droplet impact velocity and surface temperature is considered with azimuth angle, Eq. (17) yields the variation of accretion density with azimuth angle. Using a simple droplet trajectory model, we have parameterized the impact velocity as a function of the airstream velocity and azimuth angle. In addition, the surface temperature distribution has been obtained using Eqs. (1–7), assuming that $m_F = m_W$.

We assume that during fluid element motion on the rime ice structure, a fluid element may move in three perpendicular directions: in the freestream direction, $+x$, and in the two directions normal to it, $\pm y$. In addition, we assume that the probability of motion in these three possible directions is the same. For each step of a fluid element, two random numbers are generated, uniformly distributed between 0 and 1. The first determines the direction of fluid element motion, whereas the second governs its freezing. If the random number exceeds the probability of freezing, the fluid element continues its motion. If the random number is less than the freezing probability, the element freezes.

Equation (17) is not used directly to compute ice density in the model. Rather, it is used to express the freezing probability as a function of the Macklin parameter. This is done by performing numerical experiments for accretions growing on a flat surface with perpendicularly impacting fluid elements. From these experiments, a relation between the freezing probability and the average ice density has been determined, $P_n = f(\rho_I)$, in a similar fashion to Szilder and Lozowski.[11] When this relation is used in conjunction with Eq. (17), the ice density can be eliminated and the probability of freezing may be expressed as a function of the icing conditions. As in the glaze region, when a fluid element freezes, a cradle location is sought, but for rime ice it is within a circle of radius Δl. This choice of cradle domain radius is made to emulate the interstitial air gaps that arise in rime icing. It is, however, somewhat arbitrary and can only be justified for now by the reasonableness of the model simulations. The local model ice density is determined directly from the simulations based on the local ratio of occupied to unoccupied grid cells within the ice matrix.

Model Results and Discussion

In this section, we examine the ice accretion on a cylinder 2.54 cm in diameter, produced by monodispersed supercooled droplets of diameter 20 μm. The morphogenetic model simulations are performed on a two-dimensional, square lattice with a grid size Δl of 60 μm, consisting of 600 by 400 cells. The total incoming water mass is divided into a set of fluid elements, each occupying 3600 μm^2 after freezing. All computations were performed on a personal computer with Microsoft Windows 2000 operating system and an AMD Athlon XP 1.8-GHz processor with 512-MB RAM. For the present domain size, the simulation time varies between about 30 and 60 min, depending on the total number of fluid elements and the atmospheric conditions. In 60 min of CPU time, it is possible to track about 40,000 fluid elements.

We will first compare model simulations with experimental results obtained by Lozowski et al.[16] Figures 2 and 3 show predicted and experimental shapes for a nominal liquid water content

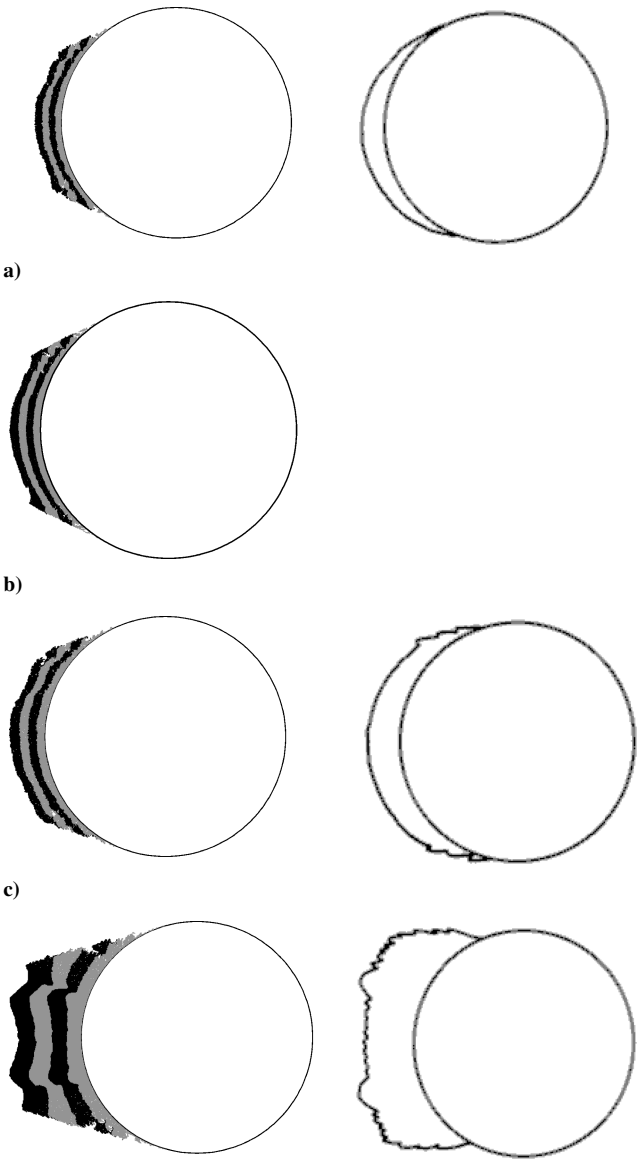

Fig. 2 Model-predicted and experimental accretion shapes for −15°C air temperature and conditions corresponding to the experiments of Lozowski et al.[16]: a) airspeed 30.5 ms^{-1}, liquid water content 0.40 gm^{-3}, icing duration 5.0 min, and grid size 60 μm; b) airspeed 30.5 ms^{-1}, liquid water content 0.40 gm^{-3}, icing duration 5.0 min, and grid size 30 μm; c) airspeed 61.0 ms^{-1}, liquid water content 0.46 gm^{-3}, and icing duration 2.5 min; and d) airspeed 122.0 ms^{-1}, liquid water content 0.44 gm^{-3}, and icing duration 2.5 min.

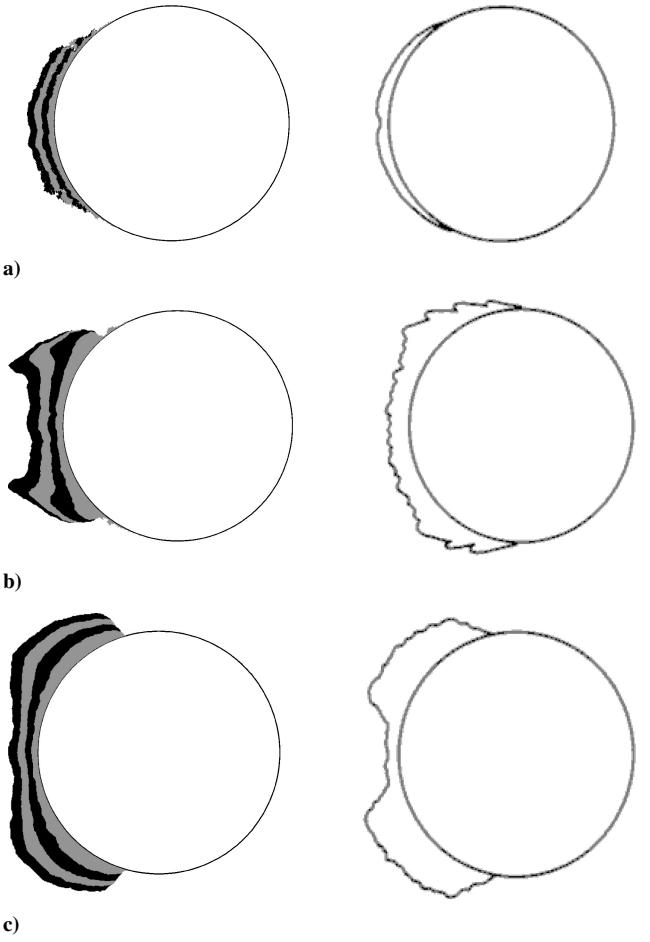

Fig. 3 Model-predicted and experimental accretion shapes for −5°C air temperature and conditions corresponding to the experiments of Lozowski et al.[16]: a) airspeed 30.5 ms^{-1}, liquid water content 0.40 gm^{-3}, and icing duration 5.0 min; b) airspeed 61.0 ms^{-1}, liquid water content 0.46 gm^{-3}, and icing duration 4.0 min; and c) airspeed 91.5 ms^{-1}, liquid water content 0.38 gm^{-3}, and icing duration 4.0 min.

of 0.4 gm^{-3} and air temperatures of −15°C and −5°C, respectively. Shading is used to distinguish four consecutive ice layers grown by the model in four equal mass increments. When the airspeed is 30.5 ms^{-1}, the model predicts that the entire ice accretion consists of rime ice (Figs. 2a and 2b). The difference between Figs. 2a and 2b is the grid resolution Δl, which is 60 μm in Fig. 2a and 30 μm in Fig. 2b. Clearly, the increased grid resolution does not have a big impact on the overall icing shape, although it does reduce the small-scale surface roughness, whereas it retains the large-scale surface roughness.

Hard rime prevails near the stagnation line, whereas a more porous ice structure may be observed away from the stagnation line. In addition, the model exhibits certain stochastic features of the ice structure such as roughness, porosity, and lack of perfect symmetry about the cylinder's horizontal axis of symmetry. The stochastic variability of the model's simulations is due to its underlying randomness. No two simulations using different sequences of random numbers are perfectly identical, even though the macroscopic conditions may be the same. We will explore the issue of model variability later. For now, however, we consider only single realizations produced by the model and compare them with single experimental realizations. Under these circumstances, the model accretion shapes generally correspond well with the experimental shapes, with some exceptions. In addition, the agreement between the stagnation line growth rates is also satisfactory (Figs. 4a and 4b).

An increase in airspeed to 61.0 ms^{-1} (Fig. 2c), leads to an increase of the impingement area. The agreement between the predicted and experimental rime ice shapes and the stagnation line growth rates is once again reasonable. When the airspeed is 122.0 ms^{-1} (Fig. 2d),

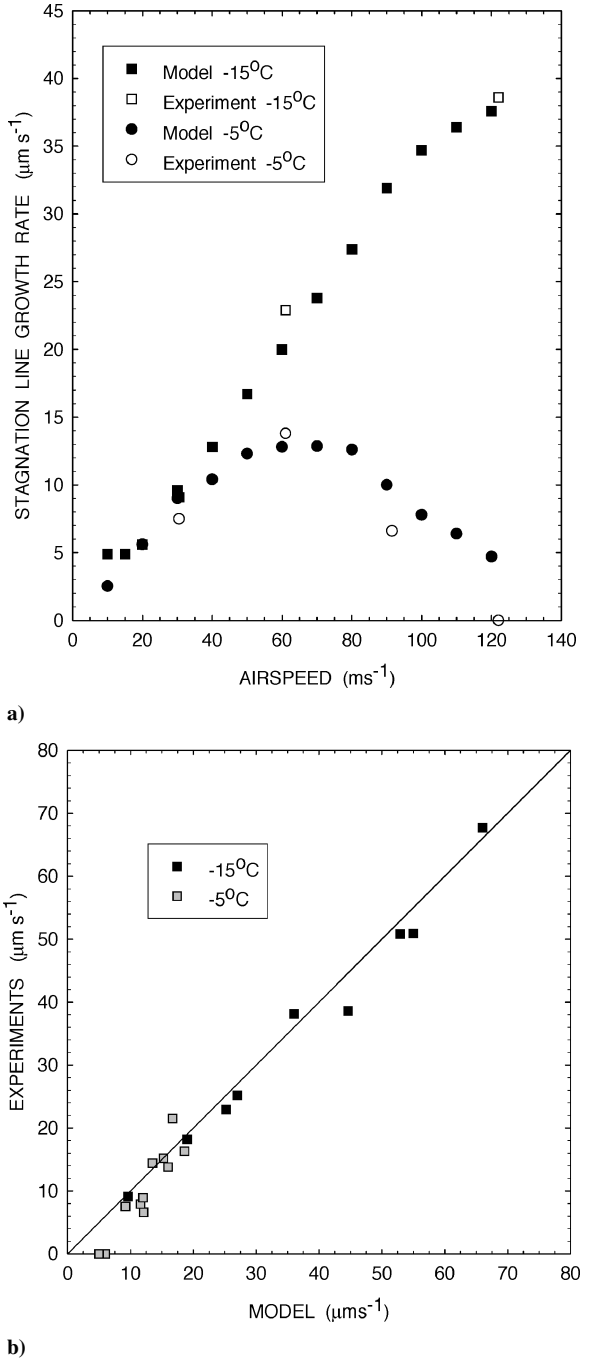

Fig. 4 Comparison of predicted and experimental stagnation line growth rate: a) stagnation line growth rate as a function of airspeed for −5 and −15°C air temperatures and b) direct comparison with the experiments of Lozowski et al.[16]

both the model simulation and the experiment exhibit glaze near the stagnations line with rime farther downstream. Water flows away from the stagnation line region leading to the formation of horns. Rime ice forms downstream from the horns. The differences between the model and experimental ice shapes may be due, in part, to the lack of recalculation of the airflow, the collection efficiency, and the heat transfer conditions during this substantial ice growth. Nevertheless, there is reasonable agreement in the stagnation line growth rates.

At an air temperature of −5°C, the extent of glaze ice increases. For an airspeed of 30.5 ms^{-1}, regions of glaze and rime coexist (Fig. 3a). The overall agreement between the model predictions and the experiments is fair. However, the model does not simulate the small depression near the leading edge (known as the stagnation line hollow) in the experiments. At an airspeed of 61.0 ms^{-1} (Fig. 3b),

the model predicts pronounced horns, whereas the experimental accretion exhibits rather small horns. This difference could be due, in part, to an incorrect distribution of the parameterized convective heat transfer coefficient, which does not account for the likelihood that the horns themselves will substantially alter the local heat transfer. Note that in the experiments there was a distribution of droplet sizes. However, in the model only a single droplet size equal to the median volume diameter of the experimental distribution was considered. This should lead to underprediction of the extent of the impingement area because larger droplets have a larger maximum impingement angle. When the airspeed is 91.5 ms^{-1} (Fig. 3c), the model shape has a somewhat greater thickness than the experimental accretion at the stagnation line, although the other glaze features are qualitatively similar.

A comparison between the model-predicted and experimental stagnation line growth rates is shown in Fig. 4a, which shows the stagnation line growth rate as a function of airspeed for a nominal liquid water content of 0.4 gm^{-3}. During the experiments, the liquid water content varied somewhat from case to case (see captions of Figs. 2 and 3), but, for consistency, all of the model results were computed for a liquid water content of 0.40 gm^{-3}. At an air temperature of $-15°C$, an increase of airspeed leads to an almost linear increase of the stagnation line growth rate. Deviations from linearity occur at airspeeds less than 20 ms^{-1}, where a gradually decreasing density characterizes the growing rime. Consequently, in this airspeed range, the stagnation line growth rate remains approximately constant. This model prediction cannot be verified with the present experimental results because airspeeds less than 30 ms^{-1} were not investigated. For airspeeds less than 105 ms^{-1}, only rime ice forms, whereas at greater airspeeds glaze ice occurs in the vicinity of the stagnation line. At high airspeeds, the aerodynamic heating term increases sufficiently to prevent total freezing at the stagnation line. Consequently, in this regime, the growth rate increases more slowly than linear with airspeed. Overall, there is encouraging agreement between the model prediction and the experimental results.

In the model, at an air temperature of $-5°C$, there is initially a similar variation of the stagnation line growth rate with airspeed. At airspeeds less than 27 ms^{-1}, rime ice forms, but its density remains close to that of glaze ice. With an increasing airspeed, as a result of aerodynamic heating, the model stagnation line growth rate reaches a maximum and then starts to diminish. The experimental results exhibit a similar qualitative behavior. For an airspeed of 122 ms^{-1}, ice accretion did not occur at the stagnation line in the experiment, but the model predicts a thin layer of glaze ice.

A more direct and comprehensive comparison between the model and experimental stagnation line growth rates is shown in Fig. 4b. All of the experimental results for air temperatures of -15 and $-5°C$ are plotted vs the model predictions for the same conditions. There is quite good agreement between the two growth rates (linear correlation coefficient 0.988), despite the somewhat higher values predicted by the model, especially when the growth rate is small.

We have also compared the morphogenetic model with other model and experimental results drawn from Ref. 19 (Fig. 5b). For this case, the discrepancy between the experimental ice shape and the simulations by all of the existing models is very substantial. All models underpredict the ice thickness over the domain where experimental ice exists. A majority of the models overpredicts the extent of the ice coverage. The morphogenetic model was run for the same conditions, and the results are presented in Fig. 5a. There is poor agreement between the simulated and experimental ice shapes. These results suggest either a general problem with all of the models or, possibly, experimental error in setting or measuring the environmental conditions.

We have used the model to analyze the influence of air temperature on the ice structure, the ice density, and the location of ice horns. At an air temperature of $-25°C$, the accretion consists entirely of rime ice (Fig. 6a). As a result of decreasing droplet impact speed and decreasing ice surface temperature with increasing azimuthal angle, the rime ice density decreases with azimuth (Fig. 7). Near the stagnation line, the rime ice density is approximately equal to the glaze ice density of 900 kgm^{-3}, decreasing rapidly to 500 kgm^{-3}, from about

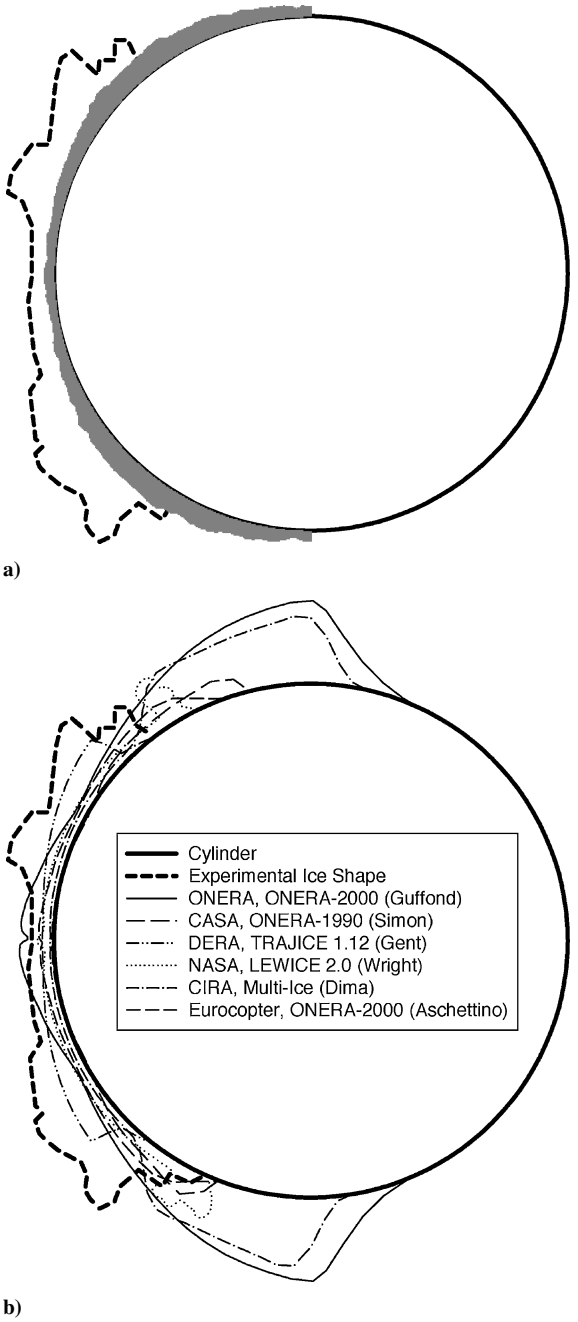

Fig. 5 Model-predicted and experimental accretion shapes for an air temperature of $-2.95°C$, airspeed 77.2 ms^{-1}, liquid water content 0.44 gm^{-3}, icing duration 5.5 min, median volume droplet diameter 18 μm, and cylinder diameter 6.35 cm: a) morphogenetic model simulation and experimental accretion shape and b) other model predictions and experimental accretion shape.

25 to 45 deg. Because of this decreasing ice density, rime ice horns form on the accretion edges. These are two-dimensional analogs of rime feathers. The changes in the model-simulated ice shape with increasing air temperature may be seen in Figs. 2a and 3a. The rime ice horns disappear, and glaze ice forms close to the stagnation line. Further air temperature increases lead to expansion of the glaze region, the formation of glaze horns, and the entire disappearance of the rime ice region at the edge of the accretion (Figs. 6b–6d). Increasing air temperature results in downstream displacement of the horn location (Fig. 8). In addition, with time, the horns tend to grow closer to the stagnation line. In Fig. 8, the maximum value is the location after the first minute, whereas the minimum value is the location after 5 min of simulation. This observation is supported qualitatively by experimental data (Fig. 9).[20] In Fig. 9, the

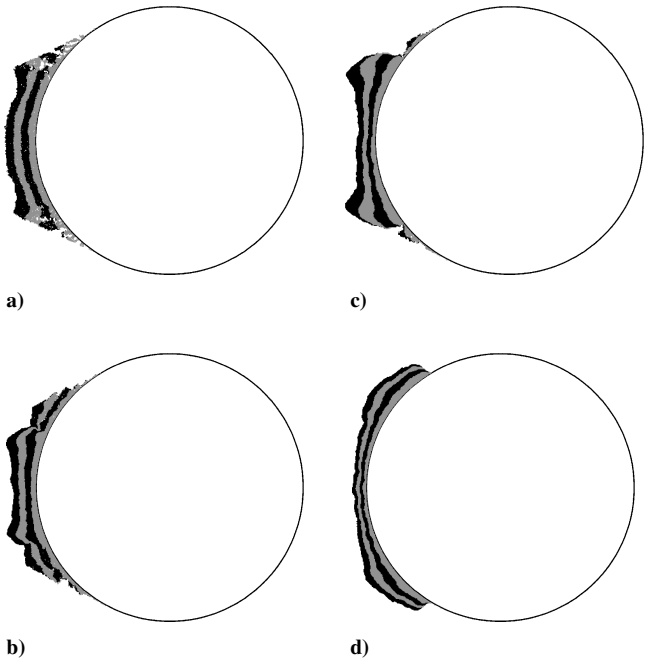

Fig. 6 Model-simulated accretion shape for an airspeed of 30.5 ms^{-1}, liquid water content of 0.40 gm^{-3}, and icing duration of 5.0 min: a) air temperature −25°C, b) air temperature −4°C, c) air temperature −3°C, and d) air temperature −2°C.

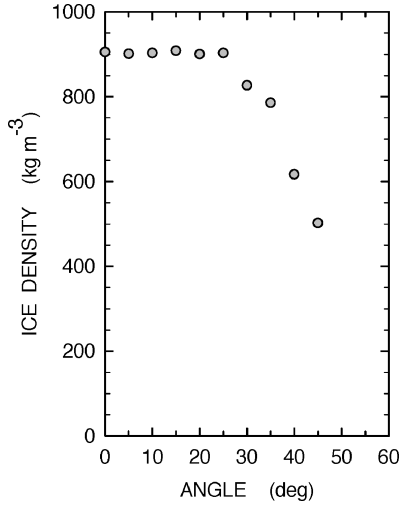

Fig. 7 Simulated ice density as a function of azimuthal angle for conditions corresponding to Fig. 6a.

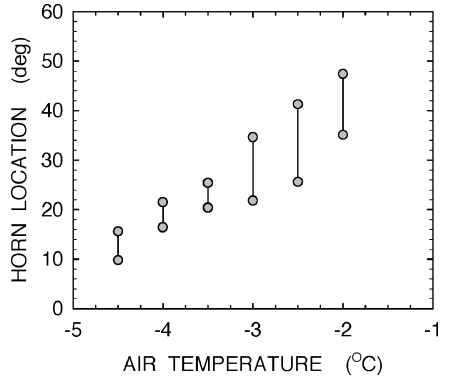

Fig. 8 Horn location as a function of air temperature for conditions corresponding to Fig. 6 and intermediate temperatures.

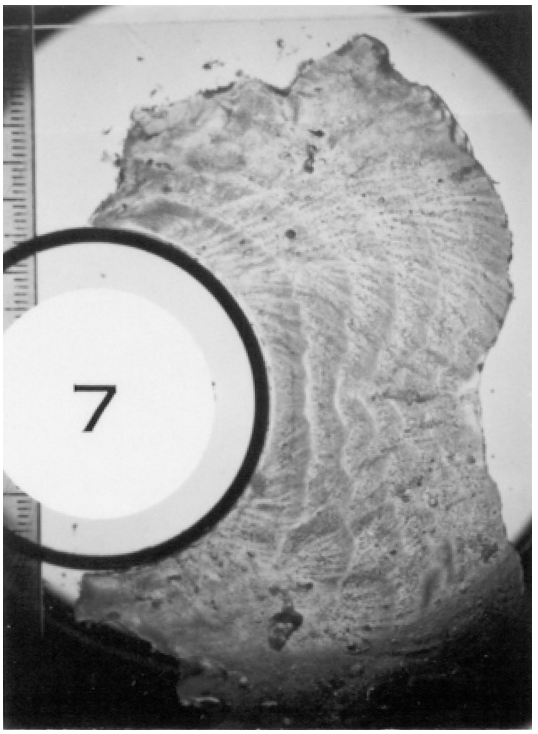

Fig. 9 Experimental ice shape[20] for air temperature −10°C, airspeed 45 ms^{-1}, liquid water content 2.09 gm^{-3}, icing duration 12 min, cylinder diameter 5.0 cm, and median droplet diameter 120 μm.

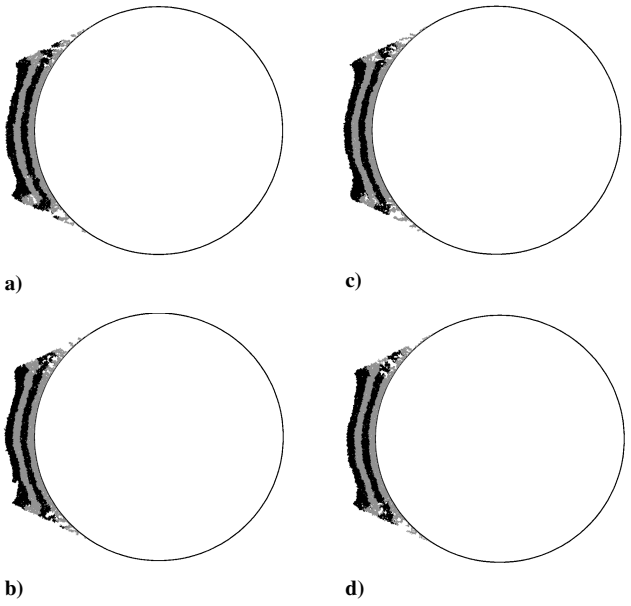

Fig. 10 Stochastic variability of the model-simulated accretion shape for an airspeed of 30.5 ms^{-1}, liquid water content of 0.40 gm^{-3}, air temperature −25°C, and icing duration of 5.0 min.

layers correspond to 2-min intervals. This experimental accretion was grown under different conditions than those of Fig. 8 but an inward migration of the maximum horn location was nonetheless observed. The model simulations also suggest that the change of horn azimuthal location during ice formation seems to be greatest at higher air temperatures.

Finally, we have also examined the variability of the model simulations. The model has been run using four different sequences of pseudorandom numbers for the conditions corresponding to Fig. 6a; other conditions were identical. It is challenging to quantify the variability of these simulations, shown in Fig. 10. Qualitatively, one may observe that the surface features of the dense rime near the stagnation

line differ from run to run. (Note the pronounced bump on the lower surface of the simulation in Fig. 10a). There is also considerable variability in the rime feathers structure, forming at the upper and lower edges of the accretion. Nevertheless, despite this stochastic variability, the overall shape and the most prominent features of the simulations, for example, horns, remain the same from run to run.

Conclusions

A two-dimensional morphogenetic model has been devised to predict both the accretion shape and the structural details and density of the ice accretion forming on a cylinder over a wide range of atmospheric and flight conditions. This allows, for the first time, to the best of our knowledge, the prediction of both the ice shape and density of aircraft ice accretions. We have produced morphogenetic model simulations of ice accretions under rime, glaze, and mixed glaze/rime conditions, as a function of the controlling parameters, air temperature, liquid water content, and airspeed. We have partially verified the model using experimental data on ice accretions forming on a cylinder under rime and glaze conditions. The results show that the morphogenetic model can simulate ice accretions on a cylinder, in reasonable agreement, qualitatively and quantitatively, with experimental data. It is difficult to assess fully the reasons for the discrepancies between model and experiment using shape alone. The experimental profiles were made using a plasticene mold in some cases or by tracing the surface outline from a photograph of a sectioned accretion. Neither technique is fully satisfactory. Because the current model resolves the internal features of the ice accretion both in space and time (whereas the original Lozowski et al.[16] model did not), it would be interesting to compare it with thin sections of experimental ice accretions, which reveal the temporal development of its crystallographic and surficial structure (similar to Fig. 9).

The results of this exploratory research are encouraging and demonstrate that morphogenetic modeling has the potential to advance the simulation of in-flight icing. In the future, we plan to use the model to simulate more accurately the time-dependent formation of ice accretion on airfoils, by recalculating the airflow, droplet trajectories, and the distribution of the convective heat transfer coefficient as the ice accretion evolves with time. This will require coupling it to airflow and droplet trajectory models. We also plan to extend the model to three dimensions, to consider the use of more appropriate lattice geometries, and to compare model variability with natural variability. Finally, it is essential to further develop morphogenetic theory to better justify the choice of arbitrary parameters and to improve the relations between microscopic model variables and macroscopic environmental and flight variables.

Acknowledgments

Edward Lozowski is grateful for an Natural Sciences and Engineering Research Council Canada Discovery Grant, which facilitated his participation in this collaborative research project. The droplet trajectory model developed by F. Fortin of the National Research Council was used to parameterize the droplet impact velocity.

References

[1]Hedde, T., and Guffond, D., "ONERA Three-Dimensional Icing Model," *AIAA Journal*, Vol. 33, No. 6, 1995, pp. 1038–1045.

[2]Wright, W. B., "Users Manual for the Improved NASA Lewis Ice Accretion Code LEWICE 1.6," NASA CR-198355, June 1995.

[3]Morency, F., Tezok, F., and Paraschivoiu, I., "Heat and Mass Transfer in the Case of Anti-Icing System Simulation," *Journal of Aircraft*, Vol. 37, No. 2, 2000, pp. 245–252.

[4]Bourgault, Y., Beaugendre, H., and Habashi, W. G., "Development of a Shallow-Water Icing Model in FENSAP-ICE," *Journal of Aircraft*, Vol. 37, No. 4, 2000, pp. 640–646.

[5]Kind, R. J., Potapczuk, M. G., Feo, A., Golia, C., and Shah, A. D., "Experimental and Computational Simulation of In-Flight Icing Phenomena," *Progress in Aerospace Sciences*, Vol. 34, Nos. 5–6, 1998, pp. 257–345.

[6]Gent, R. W., Dart, N. P., and Cansdale, J. T., "Aircraft Icing," *Philosophical Transactions of the Royal Society of London, Series A: Mathematical and Physical Sciences*, Vol. 358, 2000, pp. 2873–2911.

[7]Myers, T. G., Charpin, J. P. F., and Thompson, C. P., "Slowly Accreting Ice due to Supercooled Water Impacting on a Cold Surface," *Physics of Fluids*, Vol. 14, No. 1, 2002, pp. 240–256.

[8]Velazquez, M. T., and Hansman, R. J., "Implementation of Combined Feather and Surface-Normal Ice Growth Models in LEWICE/X," AIAA Paper 95-0753, Jan. 1995.

[9]Szilder, K., "Simulation of Ice Accretion on a Cylinder Due to Freezing Rain," *Journal of Glaciology*, Vol. 40, No. 136, 1994, pp. 586–594.

[10]Szilder, K., "The Density and Structure of Ice Accretion Predicted by a Random-Walk Model," *Quarterly Journal of the Royal Meteorological Society*, 119, 1993, pp. 907–924.

[11]Szilder, K., and Lozowski, E. P., "Three-Dimensional Modelling of Ice Accretion Density," *Quarterly Journal of the Royal Meteorological Society*, Vol. 126, 2000, pp. 2395–2404.

[12]Szilder, K., and Lozowski, E. P., "A New Method of Modelling Ice Accretion on Objects of Complex Geometry," *International Journal of Offshore and Polar Engineering*, Vol. 5, No. 1, 1995, pp. 37–42.

[13]Lozowski, E. P., Szilder, K., and Makkonen, L., "Computer Simulation of Marine Ice Accretion," *Philosophical Transactions of the Royal Society of London, Series A: Mathematical and Physical Sciences*, Vol. 358, 2000, pp. 2811–2845.

[14]Szilder, K., Lozowski, E. P., and Reuter, G., "A Study of Ice Accretion Shape on Cables Under Freezing Rain Conditions," *Transactions of the ASME, Journal of Offshore Mechanics and Arctic Engineering*, Vol. 124, No. 3, 2002, pp. 162–168.

[15]Szilder, K., and Lozowski, E. P., "A New Discrete Approach Applied to Modelling of In-Flight Icing," *Canadian Aeronautics and Space Journal*, Vol. 48, No. 3, 2002, pp. 181–193.

[16]Lozowski, E. P., Stallabrass, J. R., and Hearty, P. F., "The Icing of an Unheated, Nonrotating Cylinder. Part II: Icing Wind Tunnel Experiments," *Journal of Climate and Applied Meteorology*, Vol. 22, Dec. 1983, pp. 2063–2074.

[17]Macklin, W. C., "The Density and Structure of Ice Formed by Accretion," *Quarterly Journal of the Royal Meteorological Society*, Vol. 88, 1962, pp. 30–50.

[18]Levi, L., Nasello, O. B., and Prodi, F., "Morphology and Density of Ice Accreted on Cylindrical Collectors at Low Values of Impacting Parameter. I: Fixed Deposits," *Quarterly Journal of the Royal Meteorological Society*, Vol. 117, 1991, pp. 761–782.

[19]Kind, R. J. (ed.), *Ice Accretion Simulation Evaluation Test*, NATO RTO TR 38, Nov. 2001.

[20]de Lorenzis, B., "Time-Dependent Behaviour of Ice Accretion on a Non-Rotating Cylinder," M.Sc. Thesis, Dept. of Geography, Univ. of Alberta, Edmonton, AB, Oct. 1979, p. 92.